Experimental and theoretical study of a new CDI device for the treatment of desulfurization wastewater

Chang Liu
North China Electric Power University - Baoding Campus
Lan Ma
North China Electric Power University - Baoding Campus
Yongyi Xu
China power hua chuang electricity technology research company
Feng Wang
China power hua chuang electricity technology research company
Yu Tan
North China Electric Power University - Baoding Campus
Luyue Huang
North China Electric Power University - Baoding Campus
shuangchen Ma (msc1225@163.com)
North China Electric Power University https://orcid.org/0000-0002-9640-2957

Research Article

Keywords: capacitive deionization, desulfurization wastewater, performance experiments, theoretical model

Posted Date: June 23rd, 2021

DOI: https://doi.org/10.21203/rs.3.rs-251131/v1

Version of Record: A version of this preprint was published at Environmental Science and Pollution Research on July 31st, 2021. See the published version at https://doi.org/10.1007/s11356-021-15651-2.

Experimental and theoretical study of a new CDI device for the treatment of desulfurization wastewater

Chang Liu [1,2], Lan Ma[1,2], Yongyi Xu[3], Feng Wang[3], Yu Tan [1], Luyue Huang [1], Shuangchen Ma [1,2]*

(1 Hebei Key Lab of Power Plant Flue Gas Multi-Pollutants Control, Department of Environmental Science and Engineering, North China Electric Power University, Baoding 071003, PR China

2 MOE Key Laboratory of Resources and Environmental Systems Optimization, Beijing 102206, China

3 China Power Hua Chuang Electricity Technology Research Company Ltd.)

***Corresponding author:** Shuangchen Ma, e-mail: msc1225@163.com; tel:86-312-7525521; Fax:86-312-7525521;*

Abstract

According to the characteristics of desulfurization wastewater, A new capacitive deionization (CDI) device was designed to study the desalination characteristics of desulfurization wastewater in this paper. The experiments investigated the desalination efficiency under different conditions which find that the best desalination efficiency is achieved at a voltage of 1.2V, pH=11 and 50℃. Besides, the ion adsorption is more favorable under acidic and alkaline conditions. The anion and cation removal performance experiments showed that the order of cation removal is Mg^{2+}＞Na^{+}＞Ca^{2+}＞K^{+} and the order of anion removal is Cl^{-}＞CO_3^{2-}＞NO_3^{-}＞SO_4^{2-}＞HCO_3^{-}. The mechanism of CDI was studied and analyzed by isothermal adsorption model and COMSOL simulation software. It was found that the Freundlich model and Redlich-Peterson model have a good fit with the experimental results. The experiments show that the CDI device has excellent stability. CDI device was used to treat actual desulfurization wastewater. Furthermore, the study provides theoretical support for the industrial application of CDI for desulfurization wastewater treatment in the future.

Keywords: capacitive deionization; desulfurization wastewater; performance experiments; theoretical model

Nomenclatures

Q_0 Constant in Langmuir model（mg/g）	K_1Constant in Pseudo-first order model (g/min)
b Constant in Langmuir model（L/mg）	K_2Constant in Pseudo-second order model (g/mg*min)
C_eConcentration of adsorbate in solution at equilibrium（mg/L）	$Q_{e,i}^{exp}$Experimental value of Qe
q_e Electrical adsorption capacity at equilibrium（mg/g）	$Q_{e,i}^{cal}$Predicted value of Qe
q_t Electrical adsorption capacity at t（mg/g）	N Number of observations in the experimental Isotherm
K_F Constant in Freundlich model $(mg/g)/(mg/L)^{1/n}$	I Electric current density
n Constant in Freundlich model	P Number of parameter in regression model
K_{RP} Constant in Redlich Peterson model（L/g）	t Time（min）
a_{RP} Constant in Redlich Peterson model（L/mg）	C_0The initial concentration of the solution
B Constant in Redlich Peterson model	C_t The concentration of the solution at T
V Volume of solution（L）	C Specific capacitance
v Scan rate (mV/s)	m The quality of the adsorbent material（g）
V_c High voltage for CV	MPSDMarquardt's percent standard deviation
V_aLow voltage for CV	

1. Introduction

At present, wet limestone-gypsum flue gas desulfurization (FGD) is widely used in most coal-fired power plants and is a mature technology with high efficiency of desulfurization (Shuangchen et al. 2016). The proper treatment of FGD wastewater has been the key to achieve zero emissions from power plants (Zheng et al. 2019). Traditional treatment methods for desulfurization wastewater include chemical precipitation (Fu and Wang 2011), biological treatment technology (Huang et al. 2017), electrodialysis (Cui et al. 2017), and thermal (Luo et al. 2019; Conidi et al. 2018; Jia and Wang 2018; Lee et al. 2018) and membrane(Iaquaniello

et al. 2014; Gingerich et al. 2018; Hassan and Darwish 2014)methods. However, these methods have many problems, such as high cost, high pre-treatment requirements, easy to scale and clogging. The quality of the prepared industrial salt is difficult to guarantee and affect its application. Therefore, there is an urgent need to find a new water treatment technology to meet the needs of deep treatment of water pollution in power plants.

Capacitive deionization (CDI) is a newly emerged wastewater treatment technology in recent years (Gao et al. 2015; Anderson et al. 2010), in which ions can be captured from the water phase by simple electrostatic interactions between the ions and the electrode surface forming an electric double layer (EDL) (Hong et al. 2020). Currently, CDI has been studied in many wastewater treatments. For example, seawater (Liu et al. 2020), brackish water (Chong et al. 2018; Huo et al. 2020), nuclear power wastewater(Zhou et al. 2020) , dye wastewater (Liu et al. 2020), wastewater containing heavy metals (Bharath et al. 2019; Jin and Hu 2020; Thamilselvan et al. 2018; You et al. 2020), etc. But CDI has rarely been studied for the treatment of thermal power plant desulfurization wastewater. CDI treatment of desulfurization wastewater has significant advantages over other processes: unlike reverse osmosis and distillation, CDI does not require high pressure or high temperature so that it can flow continuously at room temperature. CDI operates under a small voltage. Compared to electrodialysis, CDI does not use ion exchange membranes, so there is no membrane fouling problem and the requirement for feed water quality is not high. Compared with membrane concentration and reduction, CDI does not require membrane replacement, has lower operating costs and is less prone to fouling and clogging. Compared with flue gas evaporation concentration technology, CDI is less prone to fouling and the flue gas concentration tower is more acidic, which can easily cause corrosion to the equipment. In addition, there is not enough space to set up desulfurization wastewater treatment device in the tail section of many power plants and the small space occupied by CDI can effectively solve such problems. Therefore, the use of CDI as a reduction unit of desulfurization wastewater to achieve zero discharge of terminal wastewater has great advantages and broad application prospects.

The system structure and adsorption materials are important factors affecting the desalination performance of CDI. As an important component of CDI, a large number of adsorbent materials have been widely studied. The current research is mainly focused on

porous carbon electrode materials with specific surface area greater than 1000 m^2/g. Carbon materials such as activated carbon, graphene, carbon spheres, carbon nanotubes, carbon fibers, porous carbon, and carbon-based aerogel are widely used in CDI electrodes because of their low cost, large specific surface area, good stability, and non-toxicity (Zhu, Wang et al. 2018). Noteworthily, as research continues, many innovative structures of CDI have emerged. For example, inverted CDI (i-CDI)、flow-through CDI、Hybrid CDI (HCDI) and Flow-electrode (FCDI). The fast proliferation of architectures available for CDI begs the question of which are the most promising. there is no clear answer as each of the architecture has unique advantages, and none should be neglected in future research work. However, the inevitable problems of any CDI structure are that the device is prone to leakage, difficult to clean, and not easy to replace and add binder resulting in lower mass transfer efficiency. The above problems have received less attention in previous studies.

Therefore, the new CDI is designed with a "pool-type" structure of outside which is prepared with plexiglass; it can effectively avoid the problem of water leakage. The electrode plates are inserted on the plexiglass instead of the traditional extrusion method. This makes it easy to replace the plates. It is noteworthy that this CDI does not add binder, and the spacing between activated carbon sponge, electrode plate and grid is reasonably controlled so that the they are closely integrated. This study designed a new type of CDI device for the water quality characteristics of desulfurization wastewater which investigated the desalination of CDI device under different conditions (voltage, pH, temperature) in order to determine the best operating conditions. Afterwards, an analysis was conducted on the removal rule of the major ions present in the desulfurization wastewater. In addition, the stability of desalination of the device was also verified experimentally which provides basic data for the application of CDI in the treatment of desulfurization wastewater.

2. Experiments

2.1 Materials

The chemicals and reagents used were purchased from Tianjin Beichen Founder Reagent Factory for analytical purity in the experiment. The raw material of the electrode plate was 316 L stainless steel. The honeycomb activated carbon sponge (from Jiangsu Maohang

Carbon Technology Co., Ltd.) was selected as the adsorption material. The pH and conductivity of the solution were tested by Hach HQ40d water quality analyzer. The solution was kept under constant temperature control by a collector thermostatic magnetic stirrer (Qiuzo DF-101S). The peristaltic pump was used by Lead Fluid (BT101L-YZ25). The power supply is an adjustable DC voltage stabilizer (MT-152D). Furthermore, the CDI device used in this experiment is self-made and the external material is plexiglass.

2.2 The design of CDI device

The CDI device designed in this experiment is designed for the characteristics of desulfurization wastewater which has large water volume and high salt content. So, it needs high flux and large adsorption capacity of CDI device. The top view and section of the device are shown in Figure 1 (a) and (b) respectively. The CDI unit is an open opening above the system which is rectangular solid, similar to a "pond". It is easy to operate and observe the water flow state. The inlet is located at the bottom of the device. The sample liquid is discharged from the top outlet on the other side of the device after it flows through the entire device so that the sample liquid can be in full contact with the adsorbent material. After the water flows into the CDI unit, there is designed a vacant zone in order to the sample can be thoroughly mixed. The plexiglass column has a recess into which the electrode plate can be mounted. This is designed for easy disassembly and replacement. The adsorption material is an activated carbon sponge which is placed close to the electrode plate. The adsorption material is separated by net. In summary, the CDI device has the features of large processing capacity, high concentration of sample liquid, easy disassembly and no water leakage.

Figure 1 Top view and section of the CDI unit

2.3 Analysis

Scanning electron microscope (SEM) (S4800 Hitachi) was used to observe the morphology of the adsorbed material. The specific surface area of nitrogen adsorption/desorption at 77.350 K at the AC electrode was determined using a surface analyzer (Auto-sorb-Iqa3200-4, Quantatech Co, USA). The cations ion content of the solution was determined using inductively coupled plasma (ICP, Optima 5300DV, Perkin Elmer) and anions ion content of the solution was determined using ion chromatograph (ICS-500, Thermo

Fisher Scientific). The surface groups of the adsorbed material were studied by FT-IR of spectrum100, PerkinElmer, Inc., USA. Electrochemical performance was tested using a CHI760E electrochemical workstation. The specific capacitance of the adsorbed material was estimated by using cyclic voltammetry (CV) which can be determined for voltages ranging from -0.6 to 1.2 V by the following equation (Liu et al. 2019):

$$C = \frac{\int_{Va}^{Vc} I\, dV}{2mv(Vc-Va)} \quad (1)$$

2.4 Desalination experiments

The cyclic sample injection was used for the test of desalination performance. Besides, the volume of sample liquid treated was 2L, as shown in Figure 2. The desorption was performed by inverted polar operation and the device was backwashed with deionized water. The concentration of the solution was calculated based on the equation between conductivity and concentration (Li et al. 2009), and the electrical adsorption capacity was calculated according to the following equation(Zhang et al. 2020):

$$q_t = \frac{(C_0-C_t)V}{m} \quad (2)$$

$$q_e = \frac{(C_0-C_e)V}{m} \quad (3)$$

Figure 2 The graph of CDI workflow

3. Result and discussion

3.1 Characterization

3.1.1 SEM and BET

Scanning electron microscope were performed in order to survey the surface morphology of the activated carbon sponge (Divyapriya et al. 2020). Figure 3 (a) and (b) show the SEM images of the activated carbon sponge without adsorbed desulfurization wastewater at low and high magnification, respectively. The activated carbon sponge has an overall coral shape with large voids and rough surface, which makes it easy for ions to adhere into the material. Figure 3(c) and (d) are SEM images of the activated carbon sponge after adsorption of desulfurization wastewater at the same magnification. It can be seen that unlike Figure 3 (a) and (b), the surface of the carbon material after the procedure is enriched with many particles, which is due to the adsorption of a large number of ions from the desulfurization wastewater.

Pore volume and specific surface area of the material was determined by

Brunauer-Emmett-Teller (BET). BET specific surface area (SBET) is given by using Brunauer-Emmett-Teller theory. In addition, the micropore volume, external surface area and micropore area is determined by the t-Plot method (Rezma et al. 2019) and the pore size distribution is used by the BJH (Barrett-Joiner- Halenda) model. Table 1 shows the test results of the activated carbon sponge. After calculated, the porosity of the adsorbent material is 22.86%. The analysis of the obtained data shows that the pore size of the material is dominated by ordered mesopores and a few micropores.

Figure 3 SEM of activated carbon sponge without adsorbed desulfurization wastewater (a) low magnification (b) high magnification; SEM of activated carbon sponge with adsorbed desulfurization wastewater (c) low magnification (d) high magnification

Table 1 Porous morphology analysis of activated carbon sponge

3.1.2 FT-IR

The FT-IR characterization was used to qualitatively detect the activated carbon sponge, and it can roughly know the surface functional groups in the adsorption material by analyzing the characteristic peaks. The results are shown in Figure 4. The characteristic peak at 2958.63cm^{-1} is caused by C-H stretching vibration of methyl (-CH_3), methylene (-CH_2) and methylene (-CH) in activated carbon sponge (Chen et al. 2005); the characteristic peak at 1728.62 cm^{-1} is related to the stretching vibration of C=O(Koch et al. 1998). Then, the characteristic peak located around the wave number 1444.19 cm^{-1} is related to the symmetric bending vibration of C-H on methyl or the deformation vibration of C-H connected to the benzene ring (Wang et al. 2014). Besides, the characteristic peak at around 1231.96 cm^{-1} is attributed to C-O bending vibration (Jaramillo et al. 2010). And the weak characteristic peaks between 700 cm^{-1} and 900 cm^{-1} are associated with C-H bending vibrations outside the plane of the aromatic ring. In conclusion, it can be seen that activated carbon sponge contains abundant surface functional groups, which can provide a large number of adsorption sites for the adsorption of pollutants. After the completion of CDI treatment, it can be observed that the wave number of the material of activated carbon sponge moves from 2958.63 cm^{-1}, 1728.62 cm^{-1}, 1444.19 cm^{-1}, 1231.96 cm^{-1}, 1016.26 cm^{-1} to 2957.81 cm^{-1}, 1728.86 cm^{-1}, 1437.61 cm^{-1},

1236.36 cm^{-1}, 1019.74 cm^{-1} respectively. It shows that the ions in solution interact with the functional groups on the surface of the material after being adsorbed.

Figure 4 FT-IR spectrum of activated carbon sponge

3.2 Electrochemical characterization

The desalination properties of CDI are related to the generation of a double layer by accumulation of ions in the electrolyte or electrolytic solution (Senoussi and Bouhidel 2018). The ion adsorption ability of the carbon electrode can be characterized by CV test(Cai et al. 2017). The CV graph of the activated carbon electrode is shown in Figure 5. A 1 M sodium chloride solution was used as the electrolyte. Besides, the scanning rates were 50 mV/s and 100 mV/s, respectively. The shape of the CV curve is almost rectangular which represents the energy storage capacity of the electrode material (Gaikwad and Balomajumder 2017). According to the calculation of Eq. (1), the specific capacitance is 67.06 F/g and 42.53 F/g at the sweep rates of 50 mV/s and 100 mV/s, respectively. In addition, no significant oxidation/reduction peaks are observed in the CV curve. This phenomenon suggests that the capacitance mainly originates from the electric double layer efficiency formed by Coulomb interactions rather than the Faraday reaction(Wang et al. 2020).

Figure 5 CV curves for sweep velocities of 50 mV/s and 100 mV/s in 1M NaCl solution

3.3 Desalination performance under different conditions

There are three experimental conditions were selected: voltage, pH and temperature in order to investigate the optimal operating conditions of the CDI device. The experiments were carried out by cyclic injection. Furthermore, NaCl solution as sample liquid, the treatment volume was 2L, and the initial concentration was 500mg/L. The treatment was carried out until the concentration no longer changed significantly. After calculation and analysis, the concentration gradient change and the electrical adsorption capacity at equilibrium are obtained.

Figure 6 shows the desalination performance of CDI at different voltages which can be found that higher voltage is better for the desalination of CDI. It is due to the electrostatic attraction will increase as the voltage increases, thereby the migration of anions and cations is

accelerated(Yang et al. 2001). The best desalination efficiency was obtained when the voltage was 1.2 V, with an electro adsorption capacity of 2.59 mg/g. It's worth noting that the desalination efficiency decreased at 1.5 V due to the hydrolysis reaction of water occurs when the applied voltage is higher than 1.23 V (Quan et al. 2017). Therefore, the optimal applied voltage for the CDI device is 1.2 V.

The pH of the solution to be treated has an important influence on the desalination performance of CDI (Zhang et al. 2019; Hassanvand et al. 2018; Hemmatifar et al. 2017). Thus, this section investigates the desalination performance of CDI at different pH. Moreover, pH was adjusted by using HCl solution and NaOH solution. The results are shown in Figure 7. CDI exerts good desalination properties under both acidic and alkaline conditions. This is a result of surface chemistry of the adsorbent material is altered under acidic or basic conditions and the surface chemistry affects the interaction between the polar or non-polar adsorbents of the activated carbon sponge. From the previous FT-IR analysis, it was shown that Na^+ and Cl^- were adsorbed and bound to functional groups on the electrode material during the adsorption process, indicating that the affinity between Na^+、Cl^- and functional groups is a key factor affecting ion desorption. As the pH increases, the carboxyl concentration decreased significantly due to the deprotonation effect. Thus, the affinity determined by the hydrogen bond strength significantly diminishes due to the decrease in the carboxyl concentration on the electrode (Wang, Chen et al. 2018). In particular, the maximum electrical adsorption capacity (3.67 mg/g) was obtained at pH = 11. The pH of the desulfurization wastewater treated by the triplex tank was alkaline. Thus, it indicates that desulfurization wastewater can be treated better by using this CDI unit.

Temperature is an important factor that cannot be neglected in the process of industrial wastewater treatment. Noteworthily, the temperature of desulfurization wastewater is generally about 45℃. For this reason, the CDI device was used to treat simulated sample liquid under isothermal conditions of 30℃～50℃ in this experiment. The results are shown in Figure 8. It can be found that the desalination capacity gradually increases with the increase of temperature, and the best desalination efficiency is obtained at 50℃. The desalination capacity of the adsorbent increases gradually with the increase of temperature. Temperature is an important factor affecting the effect of ion adsorption, which has a significant effect on the

removal rate of ions and the morphological distribution on the adsorption medium. From the experimental results, it is easy to see that the electric adsorption process is endothermic, and the increase in temperature facilitates the reaction. This may be due to the fact that as the temperature increases, the adsorbent generates new adsorption sites or the original inert active sites are activated, and it increases the probability of contact and collision between adsorbent and ions（Na^+ and Cl^-）, which accelerates the internal diffusion transport rate of Na^+ and Cl^- into the surface of the adsorbent. Thus, the increase of the active site on the adsorbent surface leads to an increase in the electrical adsorption capacity due to the increase in temperature. In addition, it also provides higher kinetic energy to increase in the ion migration rate with the increase of temperature (Huang and Tang 2020) .

Figure 6 Electrical adsorption performance at different voltages and electrical adsorption capacity at equilibrium

Figure 7 Electrical adsorption performance at different pH and electrical adsorption capacity at equilibrium

Figure 8 Electrical adsorption performance at different temperature and electrical adsorption capacity at equilibrium

3.4 Removal law of anions and cations

According to the main pollutants present in the desulfurized wastewater, K^+, Na^+, Ca^{2+}, and Mg^{2+} were selected as cations representatives. Besides, Cl^-, NO^{3-}, $SO4^{2-}$, HCO^{3-}, and CO_3^{2-} as anions representatives. In this section, the electrical adsorption properties of CDI for cations and anions were investigated at 1.2V、100mL/min and the initial ion concentration of 0.01mol/L. The results obtained are shown in Figure 9 and Figure 10, respectively. From Figure 9, it can be seen that the electrical adsorption capacity of each cation is as follows (from the largest to the smallest): Mg^{2+} (2.86mg/g) > Na^+ (2.36mg/g) > Ca^{2+} (2.34mg/g) > K^+ (2.14mg/g) when the adsorption equilibrium is reached. The hydration radius shown in Table 2. Noticeably, the maximum amount of electrical adsorption should be K^+, but this is contrary to experimental results which is consistent with the previously reported findings (Mossad and

Zou 2012; Xu et al. 2008). This phenomenon can be roughly explained from the electronegativity point of view, where the is (from largest to smallest): Mg^{2+} (1.31) > Ca^{2+} (1.00) > Na^{+} (0.93) > K^{+} (0.82). The electrical adsorption capacity of Na^{+} was slightly higher than Ca^{2+}, but the electronegativity was lower than that of Ca^{2+}, probably due to the fact that the ionic radius of Na^{+} was smaller than that of Ca^{2+} and the smaller ionic radius was easier to enter the pore structure. What's more, the electrical adsorption capacity of each anion is from largest to smallest: Cl^{-} (2.36mg/g) > CO_3^{2-} (1.74mg/g) > NO_3^{-} (1.50mg/g) > SO_4^{2-} (1.47mg/g) > HCO_3^{-} (0.98mg/g). From the experimental results, it can be seen that the best adsorption effect was obtained for Cl^{-}, which is probably due to the fact that Cl^{-} has the smallest ionic radius. For anions with the same charge, the adsorption efficiency is mainly affected by the difference of the radius. In terms of electronegativity, Cl is 3.16, which is higher than N (3.04), S (2.58) and C (2.55). It is obvious that Cl^{-} has a higher ability to attract electrons than other ions. Moreover, the increase of the active site on the adsorbent surface leads to an increase in the electrical adsorption capacity due to the increase in temperature. In combination with the hydration radius in Table 2, it was found that most of the ions conformed to this law. In particular, the higher adsorption of CO_3^{2-} may be due to the ease of binding to hydroxyl groups in solution to generate CO_2 and H_2O (Bai et al. 2019).

Figure 9 Adsorption capacity curves for different cations treated with CDI

Figure 10 Adsorption capacity curves for different anions treated with CDI

Table 2 Hydration radius of anions and cations

3.5 Adsorption Kinetics

Using pseudo first order model and pseudo second order model, the electrical adsorption process of cdi can be described. The pseudo first order model and pseudo second order model are calculated according to Eq. (4) and Eq. (5) (El-Khaiary and Malash 2011), respectively.

$$log(q_e - q_t) = log\, q_e - \frac{k_1}{2.303} t \quad (4)$$

$$q = \frac{q_e^2 kt}{1+q_e kt} \quad (5)$$

Validation of the kinetic model using the average relative error equation (ARE) (Kumar et al. 2011):

$$ARE\% = \sqrt{\sum_{i=1}^{N}\left(\frac{Q_{e,i}^{exp} - Q_{e,i}^{cal}}{Q_{e,i}^{exp}}\right)^2} \times \frac{100}{N} \quad (6)$$

The data obtained from the desalination of samples at different concentrations (100mg/L, 200mg/L, 300mg/L, 400mg/L and 500mg/L) were brought into the pseudo first order model and pseudo second order model and the results was shown in Figure 11.The parameters of the pseudo first order model and pseudo second order model are shown in Table 3.Compared to the pseudo second order model, pseudo first order model exhibits a lower ARE and a higher R^2 value. It was shown that the experimental results of the CDI device were more consistent with the pseudo first order model. It indicates that electrical adsorption process is electrostatic interactions between ions on the electrode and ions in solution, and similar conclusions were reached by prior study (Gaikwad and Balomajumder 2017b).

Figure 11 Comparison of kinetic model and experimental data

Table 3 Parameter estimation of the kinetic model

3.6 Isothermal adsorption model

Isothermal adsorption model studies focus on optimizing adsorption and understanding the driving forces that control the interaction between adsorbent and adsorbent. The Langmiur model and Freundlich model being the most commonly used, Langmiur model is based on the ideal assumption that the adsorbed surface is perfectly homogeneous. Whereas, Freundlich model being used for highly heterogeneous surfaces. The Peterson equation model is a combination of the Langmiur model and Freundlich model (OZKAYA 2006).

Langmiur model:

$$q_e = （Q_0 b C_e）/（1 + bC_e）（7）$$

Freundlich model:

$$q_e = K_F C_e^{1/n} （8）$$

Peterson equation model:

$$q_e = \frac{K_{RP} \times C_{eq}}{1 + a_{RP} \times C_{eq}^{\beta}} \quad (9)$$

MPSD is the parameter used to value the adsorption equilibrium and can be used to evaluate the isothermal model, which can be obtained by the following equation:

$$MPSD = 100 \sqrt{\frac{1}{N-P} \sum_{i=1}^{N} \left(\frac{Q_{e,i}^{exp} - Q_{e,i}^{cal}}{Q_{e,i}^{exp}} \right)^2} \quad (10)$$

The Langmuir, Freundlich and Redlich Peterson isothermal models are used to fit the obtained experimental results. Figure 12 shows the fitting results of the three isothermal adsorption models, and the obtained parameter estimates are shown in Table 4. It can be seen that the Freundlich and Redlich-Peterson models fit better with the experimental results by comparing the R^2 and MPSD. Because they have higher R^2 and lower MPSD values. This may be owing to the fact that the adsorption of ions by activated carbon sponge is a multimolecular layer adsorption. Indeed, the adsorption material is a mesoporous dominated carbon material which contributes to the pore adsorption.

Figure 12 Comparison of three adsorption isotherm models

Table 4 Parameter estimation of three adsorption isotherm models

3.7 COMSOL analysis of rectangular CDI unit

Computer simulation has proven to be one of the most technically advantageous methods for solving a variety of engineering problems. CFD provide a great deal of information about the flow of fluids as well as the simulation details of the geometry. It also allows for easy parameter changes which makes them very powerful design systems (Sousa et al. 2014). In this paper, COMSOL Multiphysics 5.5 software is used to analyze the fluid flow behavior during the desalination process of CDI. Set the CDI as a rectangular structure with a size of 50cm×10cm×2cm, the inlet and outlet are located at the center of the narrow side, and the aperture is 1cm. Figure 13 shows the velocity profiles of the CDI rectangular flow channel at different flow rates. It can be seen that the velocities on the outside are higher than the

velocities on the inside at high flow rates unlike some previous reports (Gaikwad et al. 2020; Jeon et al. 2017). That means that the distribution of the solution is not uniform so that the desalination efficiency of the outside of the CDI is higher than that of the inside. This may cause the outside to reach adsorption saturation and the inside is still unsaturated. But a large amount of solution passes through the outside for which there is a decrease in the overall desalination efficiency. Furthermore, the flow field is more evenly distributed in the case of low flow rate which enables efficient desalination of each part. It also reveals that large dead zones appear at the corners and eddy current is produced at high flow rates from the flow distribution graph (Figure 14).

Figure 13 Velocity profiles of rectangular CDI flow paths at different flow rates: (a) 100mL/min, (b) 200mL/min, (c) 300mL/min, (d) 400mL/min, and (e) 500mL/min

Figure 14 Streamlines profile of rectangular CDI flow paths at different flow rates: (a) 100mL/min, (b) 200mL/min, (c) 300mL/min, (d) 400mL/min, (e) 500mL/min

3.8 Stability of CDI desalination performance

The long-term stability of the system is an important indicator to test the performance of the CDI device (Wang et al. 2020; Moustafa et al. 2020; Wang et al. 2018). In this experiment, a NaCl solution with an initial concentration of 500 mg/L was selected and continuously adsorbed and desorbed 10 times under a voltage of 1.2V. The adsorption and desorption were performed by inverted polarity operation and rinsed with deionized water. The time ratio of adsorption and desorption is 1:1. Figure 15 shows the conductivity change of the CDI device with 10 cycles of desalination. It can be seen that the downward trend of the CDI device during the 10 runs is approximately the same with the conductivity dropping from about 1000 μs/cm to about 850 μs/cm. Therefore, the CDI device has a good stability of desalination performance.

Figure 15 Electrical adsorption performance of CDI unit during 10 cycles

3.9 Desalination efficiency of actual desulfurization wastewater

Desulfurization wastewater generally has high salt、hardness content and is prone to

scaling which is due to the high content of Ca^{2+}, Mg^{2+}, Na^{+} and suspended particulate matter. And the desulfurization wastewater weakly acidic and corrosive is caused by higher content of Cl^{-}. For this reason, the CDI device was used for treating actual desulfurization wastewater focusing on the removal effect of the main ions contained. The water sample is selected from the desulfurization wastewater of a power plant after the triple tank treatment. The sample was diluted five times and then used as the solution to be treated. 2 L of the solution to be treated was injected in a cyclic manner and the real-time desalination effect was observed and recorded. The change of and electrical adsorption capacity are shown in Figure 16. It can be seen that the conductivity is decreased after treatment, the removal effect on the high concentration of desulfurization wastewater is not very satisfactory which is may owing to the small size of the device. Afterwards, the main anions and cations present in the treated sample liquid were detected. Table 5 records the values of each index in the desulfurization wastewater (before and after treatment). By comparing the changes of ions before and after treatment, it is found that the removal of Ca^{2+}, Na^{+} and Cl^{-} is relatively good which is consistent with the conclusions of previous experiments. Rather surprisingly, the water samples selected for this study contained less Mg^{2+} which is not a reference value. In addition, there is a corresponding decrease in TDS as well as pH value.

Figure 16 Conductivity and electrical adsorption capacity of CDI treatment of actual desulfurization wastewater

Table 5 Comparison of values of indicators in desulfurization wastewater before and after treatment

4. Conclusions

In this paper, the following conclusions are drawn from the study of a new CDI unit for the treatment of desulfurization wastewater.

(1) Activated carbon sponge was selected as the adsorption material and characterized by SEM, BET, FT-IR and CV tests. The results show that it has good pore structure、large specific surface area (27.4536 m^2/g) and good specific capacitance (67.06F/g) is obtained at a

sweep speed of 50mV/s.

(2) The desalination was investigated under different voltage, temperature and pH conditions. Consequently, the best desalination efficiency is obtained at 1.2V, 50℃ and pH=11. In addition, this study also found that the desalination and adsorption were more effective under acidity or alkalinity conditions. Furthermore, the removal efficiency of different anions and cations was investigated. The results indicate that the final electro adsorption capacities were as follows: Mg^{2+}＞Na^{+}＞Ca^{2+}＞K^{+} and Cl^{-}＞CO_3^{2-}＞NO_3^{-}＞SO_4^{2-} ＞HCO_3^{-}.

(3) The adsorption kinetics and isothermal adsorption models were studied and analyzed. It was concluded that the experimental results of the CDI device were more consistent with the pseudo first order model. Furthermore, the Freundlich and Redlich-Peterson models are better fitted with the experimental results. The CDI device designed have dead zones at high flow rates in this paper. In other words, low flow rates are more favorable for desalination through COMSOL software simulation.

(4) According to the requirements of practical applications, the stability of the CDI device was tested in several sets of desalination experiments. Consequently, the experimental results showed that the stability of the device is excellent. In addition, the CDI device was also used to treat actual desulfurization wastewater so that the device exhibited a certain desalination capacity.

Acknowledgement

This work was supported by the financial support of National Key R&D Program of China (2018YFB0604305-01).

Authors Contributions：

Shuangcheng Ma，Chang Liu and Lan Ma wrote the main manuscript text，Yongyi Xu and Feng Wang participated in the design of the experiment，Yu Tan modified this article, and Dingchang Yang translated the language of the article.

Competing Interests:

(1) The authors have no relevant financial or non-financial interests to disclose.

(2) The authors have no conflicts of interest to declare that are relevant to the content of this article.

(3) All authors certify that they have no affiliations with or involvement in any organization or entity with any financial interest or non-financial interest in the subject matter or materials discussed in this manuscript.

(4) The authors have no financial or proprietary interests in any material discussed in this article.

Ethical Approval:

The manuscript has not been published before or submitted to another journal for the consideration of publication. And all contents in this article is original.

Consent to Participate

Not applicable

Consent to Publish section

We approve themanuscript to be published

Availability of data and materials

All data generated or analysed during this study are included in this published article.

References:

Anderson, M. A., Cudero, A. L., and Palma, J. (2010). "Capacitive deionization as an electrochemical means of saving energy and delivering clean water. Comparison to present desalination practices: Will it compete?" Electrochimica acta, 55(12), 3845-3856. doi: 10.1016/ j. electacta. 2010. 02.012.

Bai, Z., Hu, C., Liu, H., and Qu, J. (2019). "Selective adsorption of fluoride from drinking water using NiAl-layered metal oxide film electrode." Journal of colloid and interface science, 539, 146-151. doi: 10.1016/j.jcis.2018.12.062.

Bharath, G., Rambabu, K., Banat, F., Hai, A., Arangadi, A. F., and Ponpandian, N. (2019). "Enhanced electrochemical performances of peanut shell derived activated carbon and its Fe3O4 nanocomposites for capacitive deionization of Cr(VI) ions." The Science of the total environment, 691, 713-726. doi:10.1016/j.scitotenv.2019.07.069.

Cai, W., Yan, J., Hussin, T., and Liu, J. (2017). "Nafion-AC-based asymmetric capacitive deionization."

Electrochimica acta, 225, 407-415.doi: 10.1016/j.electacta.2016.12.069.
Chen, B., Johnson, E. J., Chefetz, B., Zhu, L., and Xing, B. (2005). "Sorption of Polar and Nonpolar Aromatic Organic Contaminants by Plant Cuticular Materials: Role of Polarity and Accessibility." Environmental science & technology, 39(16), 6138-6146. doi: 10.1021/es050622q.
Chong, L. G., Chen, P. A., Huang, J. Y., Huang, H. L., and Wang, H. P. (2018). "Capacitive deionization of a RO brackish water by AC/graphene composite electrodes." Chemosphere (Oxford), 191, 296-301. doi:10.1016/j.chemosphere.2017.10.064.
Conidi, C., Macedonio, F., Ali, A., Cassano, A., Criscuoli, A., Argurio, P., and Drioli, E. (2018). "Treatment of Flue Gas Desulfurization Wastewater by an Integrated Membrane-Based Process for Approaching Zero Liquid Discharge." Membranes (Basel), 8(4), 117. doi: 10.3390/ membranes 8040117.
Cui, L., Li, G., Li, Y., Yang, B., Zhang, L., Dong, Y., and Ma, C. (2017). "Electrolysis-electrodialysis process for removing chloride ion in wet flue gas desulfurization wastewater (DW): Influencing factors and energy consumption analysis." Chemical engineering research & design, 123, 240-247. doi: 10.1016/j.cherd.2017.05.016.
Divyapriya, G., Kumar, K. V., Rajesh, L., and Nambi, I. M. (2020). "Electro-enhanced removal of perchlorate ions from aqueous solution using capacitive deionization process." Journal of industrial and engineering chemistry (Seoul, Korea), 89, 351-360. doi: 10.1016/j.jiec.2020.06.002.
El-Khaiary, M., I., and Malash, G., F. (2011). "Common data analysis errors in batch adsorption studies."Hydrometallurgy 105(3-4): 314-320. doi: 10.1016/j.hydromet.2010.11.005.
Fu, F., and Wang, Q. (2011). "Removal of heavy metal ions from wastewaters: A review." Journal of environmental management, 92(3), 407-418. doi: 10.1016/j.jenvman.2010.11.011.
Gaikwad, M. S., Balomajumder, C., and Tiwari, A. K. (2020). "Acid treated RHWBAC electrode performance for Cr(VI) removal by capacitive deionization and CFD analysis study." Chemosphere (Oxford), 254, 126781-126781.doi: 10.1016/j.chemosphere.2020.126781.
Gaikwad, M. S., and Balomajumder, C. (2017a). "Simultaneous electrosorptive removal of chromium(VI) and fluoride ions by capacitive deionization (CDI): Multicomponent isotherm modeling and kinetic study." Separation and purification technology, 186, 272-281. doi: 10.1016/ j.seppur. 2017.06.017.
Gaikwad, M. S., and Balomajumder, C. (2017b). "Simultaneous electrosorptive removal of chromium(VI) and fluoride ions by capacitive deionization (CDI): Multicomponent isotherm modeling and kinetic study." Separation and purification technology, 186, 272-281. doi: 10.1016/ j.seppur. 2017.06.017.
Gao, X., Omosebi, A., Landon, J., and Liu, K. (2015). "Surface charge enhanced carbon electrodes for stable and efficient capacitive deionization using inverted adsorption-desorption behavior." Energy & environmental science, 8(3), 897-909. doi: 10.1039/c4ee03172e.
Gingerich, D. B., Bartholomew, T. V., Mauter, M. S., and Carnegie Mellon Univ., P. P. U. S. (2018). "Technoeconomic Optimization of Emerging Technologies for Regulatory Analysis." ACS sustainable chemistry & engineering, 6(2), 2370-2378.doi:10.1021/acssuschemeng.7b03821.
Hassan, A. S., and Darwish, M. A. (2014). "Performance of thermal vapor compression." Desalination, 335(1), 41-46.doi: 10.1016/j.desal.2013.12.004.
Hassanvand, A., Chen, G. Q., Webley, P. A., and Kentish, S. E. (2018). "A comparison of multicomponent electrosorption in capacitive deionization and membrane capacitive deionization." Water research (Oxford), 131, 100-109. doi: 10.1016/j.watres.2017.12.015.

Hemmatifar, A., Oyarzun, D. I., Palko, J. W., Hawks, S. A., Stadermann, M., Santiago, J. G., and Lawrence Livermore National Lab. LLNL, L. C. U. S. (2017). "Equilibria model for pH variations and ion adsorption in capacitive deionization electrodes." Water research (Oxford), 122(C), 387-397. doi: 10.1016/j.watres.2017.05.036.

Hong, S. P., Yoon, H., Lee, J., Kim, C., Kim, S., Lee, J., Lee, C., and Yoon, J. (2020). "Selective phosphate removal using layered double hydroxide/reduced graphene oxide (LDH/rGO) composite electrode in capacitive deionization." Journal of colloid and interface science, 564, 1-7. doi:10.1016 / j.jcis.2019.12.068 .

Huang, K. Z., and Tang, H. L. (2020). "Temperature and desorption mode matter in capacitive deionization process for water desalination." Environmental technology, 41(26), 3456-3463.doi: 10. 1080/09593330.2019.1611941

Huang, Y., Chen, Y., Guo, X., and Zheng, C. (2017). "Experimental study on the stability of the ClHgSO3 − in desulfurization wastewater." Environmental science and pollution research international, 24(20), 17031-17040. doi: 10.1007/s11356-017-9359-9.

Huo, S., Song, X., Zhao, Y., Ni, W., Wang, H., and Li, K. (2020). "Insight into the significant contribution of intrinsic carbon defects for the high-performance capacitive desalination of brackish water." Journal of materials chemistry. A, Materials for energy and sustainability, 8(38), 19927-19937. doi: 10.1039/d0ta07014a.

Iaquaniello, G., Salladini, A., Mari, A., Mabrouk, A. A., and Fath, H. E. S. (2014). "Concentrating solar power (CSP) system integrated with MED–RO hybrid desalination." Desalination, 336(1), 121-128. doi: 10.1016/j.desal.2013.12.030.

Jaramillo, J., Álvarez, P. M., and Gómez-Serrano, V. (2010). "Oxidation of activated carbon by dry and wet methods surface chemistry and textural modifications." Fuel processing technology, 91(11), 1768-1775. doi: 10.1016/j.fuproc.2010.07.018.

Jeon, Y. S., Cheong, S. I., and Rhim, J. W. (2017). "Design shape of CDI cell applied with APSf and SPEEK and performance in MCDI." Macromolecular research, 25(7), 712-721. doi: 10.1007 /s 13233 - 017-5064-2.

Jia, F., and Wang, J. (2018). "Treatment of flue gas desulfurization wastewater with near-zero liquid discharge by nanofiltration-membrane distillation process." Separation science and technology, 53(1), 146-153. doi: 10.1080/01496395.2017.1379539.

Jin, W., and Hu, M. (2020). "Cobalt oxide, sulfide and phosphide-decorated carbon felt for the capacitive deionization of lead ions." Separation and purification technology, 237, 116343. doi: 10. 1016/j.seppur.2019.116343.

Koch, A., Krzton, A., Finqueneisel, G., Heintz, O., Weber, J., and Zimny, T. (1998). "A study of carbonaceous char oxidation in air by semi-quantitative FTIR spectroscopy." Fuel (Guildford), 77(6), 563-569. doi: 10.1016/S0016-2361(97)00157-9.

Kumar, S., Zafar, M., Prajapati, J. K., Kumar, S., and Kannepalli, S. (2011). "Modeling studies on simultaneous adsorption of phenol and resorcinol onto granular activated carbon from simulated aqueous solution." Journal of hazardous materials, 185(1), 287-294. doi: 10.1016/j.jhazmat. 2010. 09 032.

Lee, S., Kim, Y., and Hong, S. (2018). "Treatment of industrial wastewater produced by desulfurization process in a coal-fired power plant via FO-MD hybrid process." Chemosphere (Oxford), 210, 44-51. doi: 10.1016/j.chemosphere.2018.06.180.

Li, H., Lu, T., Pan, L., Zhang, Y., and Sun, Z. (2009). "Electrosorption behavior of graphene in NaCl

576 solutions." Journal of materials chemistry, 19(37), 6773-6779. doi: 10.1039/b907703k.
577 Liu, G., Qiu, L., Deng, H., Wang, J., Yao, L., and Deng, L. (2020). "Ultrahigh surface area carbon
578 nanosheets derived from lotus leaf with super capacities for capacitive deionization and dye
579 adsorption." Applied surface science, 524, 146485. doi: 10.1016/j.apsusc.2020.146485.
580 Liu, H., Zhang, J., Xu, X., and Wang, Q. (2020). "A Polyoxometalate-Based Binder-Free Capacitive
581 Deionization Electrode for Highly Efficient Sea Water Desalination." Chemistry : a European journal,
582 26(19), 4403-4409. doi: 10.1002/chem.201905606.
583 Liu, N., Sun, S., and Hou, C. (2019). "Studying the electrosorption performance of activated carbon
584 electrodes in batch-mode and single-pass capacitive deionization." Separation and purification
585 technology, 215, 403-409. doi: 10.1016/j.seppur.2019.01.029.
586 Luo, Z., Wang, D., Zhu, D., Xu, J., Jiang, H., Geng, W., Wei, W., and Lian, Z. (2019). "Separation of
587 fluoride and chloride ions from ammonia-based flue gas desulfurization slurry using a two-stage
588 electrodialysis." Chemical engineering research & design, 147, 73-82. doi:10.1016/j.cherd. 2019.
589 05.003.
590 Mossad, M., and Zou, L. (2012). "A study of the capacitive deionisation performance under various
591 operational conditions." Journal of hazardous materials, 213-214, 491-497. doi: 10.1016/ j.jhazmat.
592 2012.02.036.
593 Moustafa, H. M., Obaid, M., Nassar, M. M., Abdelkareem, M. A., and Mahmoud, M. S. (2020).
594 "Titanium dioxide-decorated rGO as an effective electrode for ultrahigh-performance capacitive
595 deionization." Separation and purification technology, 235,116178. doi:10.10 /j.seppur.2019.11617 8.
596 OZKAYA, B. (2006). "Adsorption and desorption of phenol on activated carbon and a comparison of
597 isotherm models." Journal of hazardous materials, 129(1-3), 158-163.doi:10.1016/ j.jhazmat.
598 2005.08.025.
599 Quan, X., Fu, Z., Yuan, L., Zhong, M., Mi, R., Yang, X., Yi, Y., and Wang, C. (2017). "Capacitive
600 deionization of NaCl solutions with ambient pressure dried carbon aerogel microsphere electrodes."
601 RSC advances, 7(57), 35875-35882. doi: 10.1039/c7ra05226j.
602 Rezma, S., Assaker, I. B., Litaiem, Y., Chtourou, R., Hafiane, A., and Deleuze, H. (2019). "Microporous
603 activated carbon electrode derived from date stone without use of binder for capacitive deionization
604 application." Materials research bulletin, 111, 222-229. doi: 10.1016 /j. materresbull. 2018.11.030.
605 Senoussi, H., and Bouhidel, K. E. (2018). "Feasibility and optimisation of a batch mode capacitive
606 deionization (BM CDI) process for textile cationic dyes (TCD) removal and recovery from industrial
607 wastewaters." Journal of cleaner production, 205, 721-727. doi: 10.1016/j.jclepro.2018.09.026.
608 Shuangchen, M., Jin, C., Gongda, C., Weijing, Y., and Sijie, Z. (2016). "Research on desulfurization
609 wastewater evaporation: Present and future perspectives." Renewable & sustainable energy reviews,
610 58, 1143-1151.doi: 10.1016/j.rser.2015.12.252.
611 Sousa, P., Soares, A., Monteiro, E., and Rouboa, A. (2014). "A CFD study of the hydrodynamics in a
612 desalination membrane filled with spacers." Desalination, 349, 22-30. doi: 10.1016/j.desal. 2014.
613 06.019.
614 Thamilselvan, A., Govindan, K., Nesaraj, A. S., Maheswari, S. U., Oren, Y., Noel, M., and James, E. J.
615 (2018). "Investigation on the effect of organic dye molecules on capacitive deionization of sodium
616 sulfate salt solution using activated carbon cloth electrodes." Electrochimica acta, 279, 24-33.
617 doi:10.1016/j.electacta.2018.05.053.
618 Wang, C., Chen, L., Liu, S., and Zhu, L. (2018). "Nitrite desorption from activated carbon fiber during
619 capacitive deionization (CDI) and membrane capacitive deionization (MCDI)." Colloids and Surfaces

A: Physicochemical and Engineering Aspects 559: 392-400. doi:10.1016/j.colsurfa.2018.09.072.

Wang, G., Yan, T., Zhang, J., Shi, L., and Zhang, D. (2020). "Trace-Fe-Enhanced Capacitive Deionization of Saline Water by Boosting Electron Transfer of Electro-Adsorption Sites." Environmental science & technology, 54(13), 8411-8419. doi: 10.1021/acs.est.0c01518.

Wang, M., Xu, X., Li, Y., Lu, T., and Pan, L. (2018). "Enhanced desalination performance of anion-exchange membrane capacitive deionization via effectively utilizing cathode oxidation." Desalination, 443, 221-227. doi: 10.1016/j.desal.2018.06.002.

Wang, S., Lin, H., Ru, B., Sun, W., Wang, Y., and Luo, Z. (2014). "Comparison of the pyrolysis behavior of pyrolytic lignin and milled wood lignin by using TG–FTIR analysis." Journal of analytical and applied pyrolysis, 108, 78-85. doi: 10.1016/j.jaap.2014.05.014.

Wang, T., Liang, H., Bai, L., Liu, B., Zhu, X., Wang, J., Xing, J., Ren, N., and Li, G. (2020). "Desalination Performance and Fouling Mechanism of Capacitive Deionization: Effects of Natural Organic Matter." Journal of the Electrochemical Society, 167(4), 43501. doi: 10.1149/1945-7111 /ab7177.

Xu, P., Drewes, J. E., Heil, D., and Wang, G. (2008). "Treatment of brackish produced water using carbon aerogel-based capacitive deionization technology." Water research (Oxford), 42(10-11), 2605-2617. doi: 10.1016/j.watres.2008.01.011.

Yang, K., Ying, T., Yiacoumi, S., Tsouris, C., and Vittoratos, E. S. (2001). "Electrosorption of Ions from Aqueous Solutions by Carbon Aerogel: An Electrical Double-Layer Model." Langmuir, 17(6), 1961-1969. doi: 10.1021/la001527s.

You, S., Tasi, C., Millet, P., and Doong, R. (2020). "Electrochemically capacitive deionization of copper (II) using 3D hierarchically reduced graphene oxide architectures." Separation and purification technology, 251, 117368. doi: 10.1016/j.seppur.2020.117368.

Zhang, C., He, D., Ma, J., Tang, W., and Waite, T. D. (2019). "Comparison of faradaic reactions in flow-through and flow-by capacitive deionization (CDI) systems." Electrochimica acta, 299, 727-735. doi: 10.1016/j.electacta.2019.01.058.

Zhang, Y., Ji, L., Zheng, Y., Liu, H., and Xu, X. (2020). "Nanopatterned metal–organic framework electrodes with improved capacitive deionization properties for highly efficient water desalination." Separation and purification technology, 234, 116124. doi: 10.1016/j.seppur.2019.116124.

Zheng, C., Zheng, H., Yang, Z., Liu, S., Li, X., Zhang, Y., Weng, W., and Gao, X. (2019). "Experimental study on the evaporation and chlorine migration of desulfurization wastewater in flue gas." Environmental science and pollution research international, 26(5), 4791-4800. doi: 10.1007/ s11356-018-3816-y.

Zhu, G., H., Wang, H., Xu, H., and Zhang, L. (2018). "Enhanced capacitive deionization by nitrogen-doped porous carbon nanofiber aerogel derived from bacterial-cellulose." Journal of Electroanalytical Chemistry 822: 81-88.

Zhou, J., Zhou, H., Zhang, Y., Wu, J., Zhang, H., Wang, G., and Li, J. (2020). "Pseudocapacitive deionization of uranium(VI) with WO3/C electrode." Chemical engineering journal (Lausanne, Switzerland : 1996), 398, 125460. doi: 10.1016/j.cej.2020.125460.

Figures

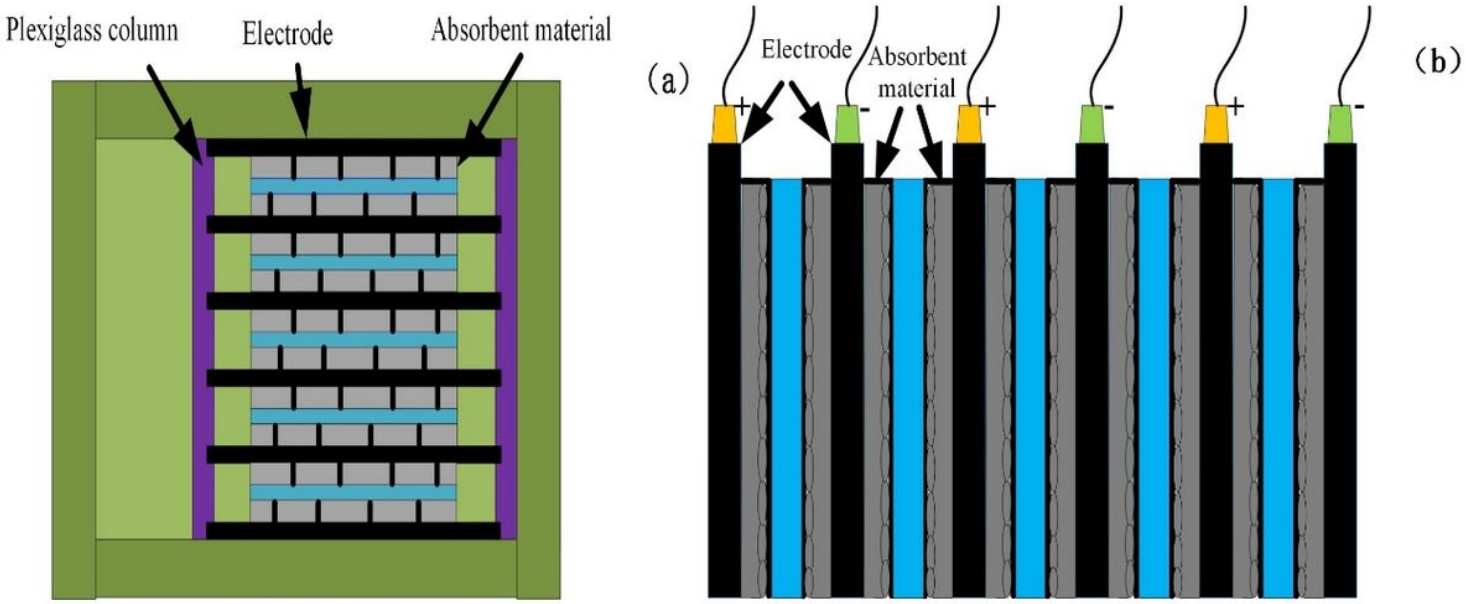

Figure 1

Top view and section of the CDI unit

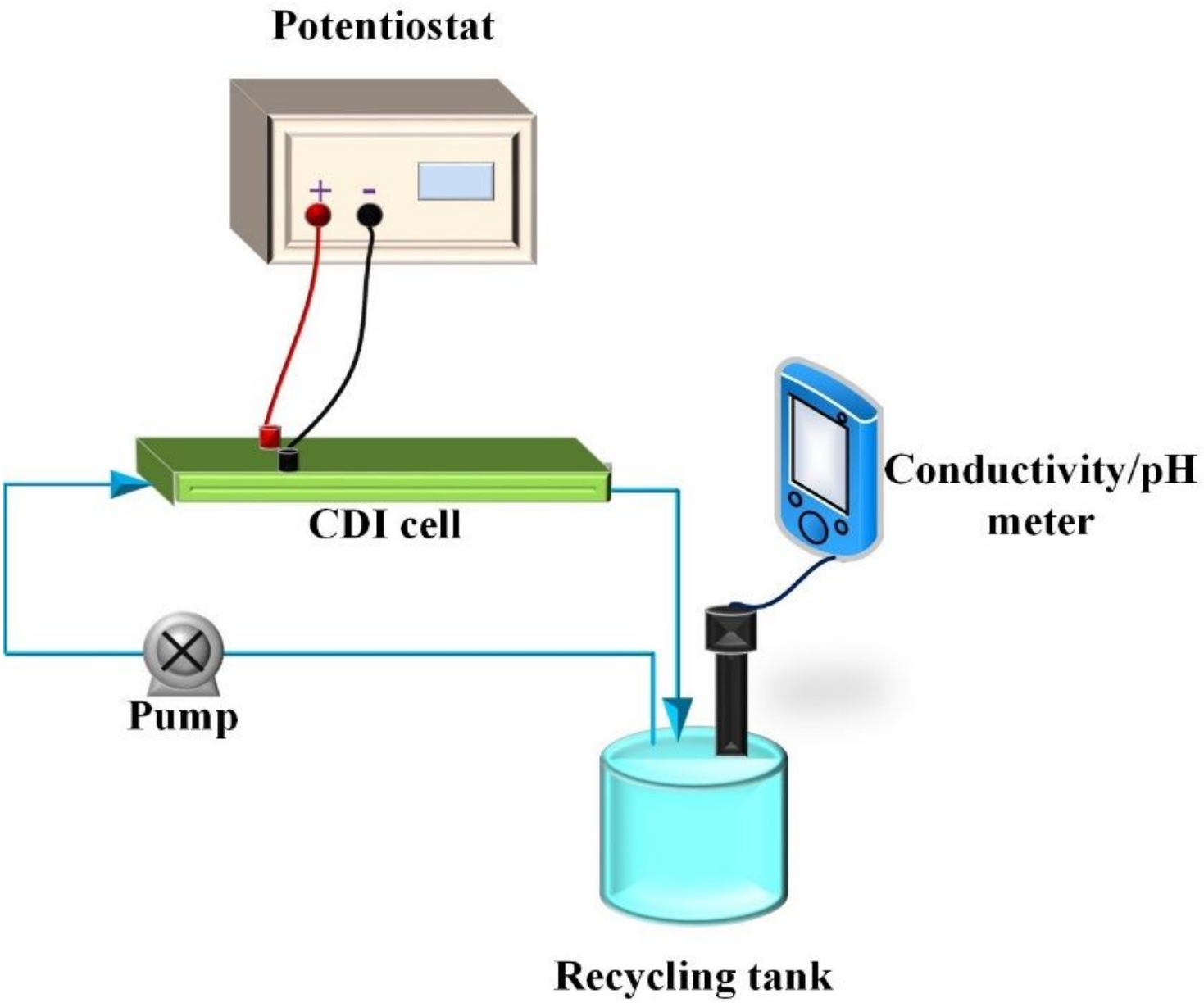

Figure 2

The graph of CDI workflow

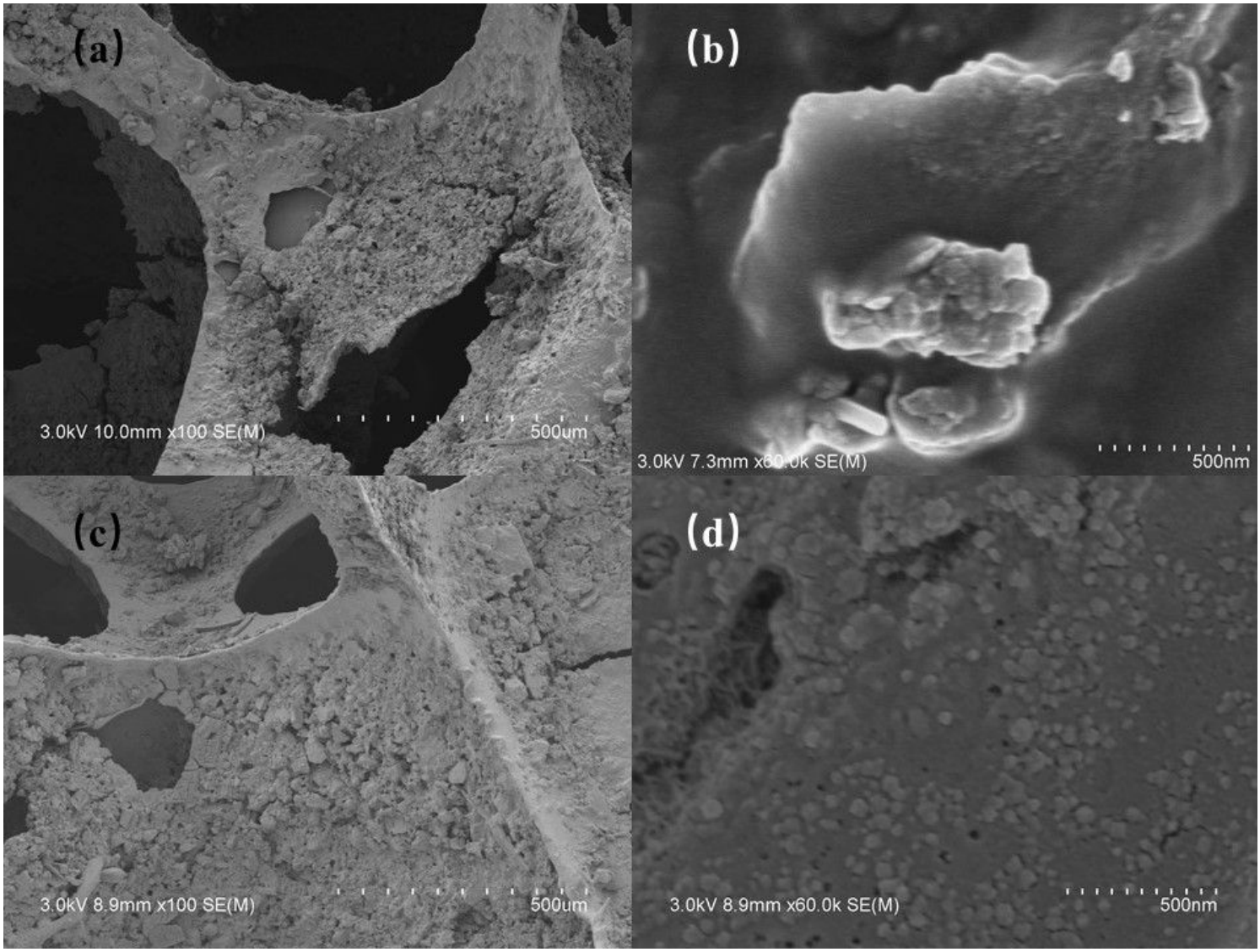

Figure 3

SEM of activated carbon sponge without adsorbed desulfurization wastewater (a) low magnification (b) high magnification; SEM of activated carbon sponge with adsorbed desulfurization wastewater (c) low magnification (d) high magnification

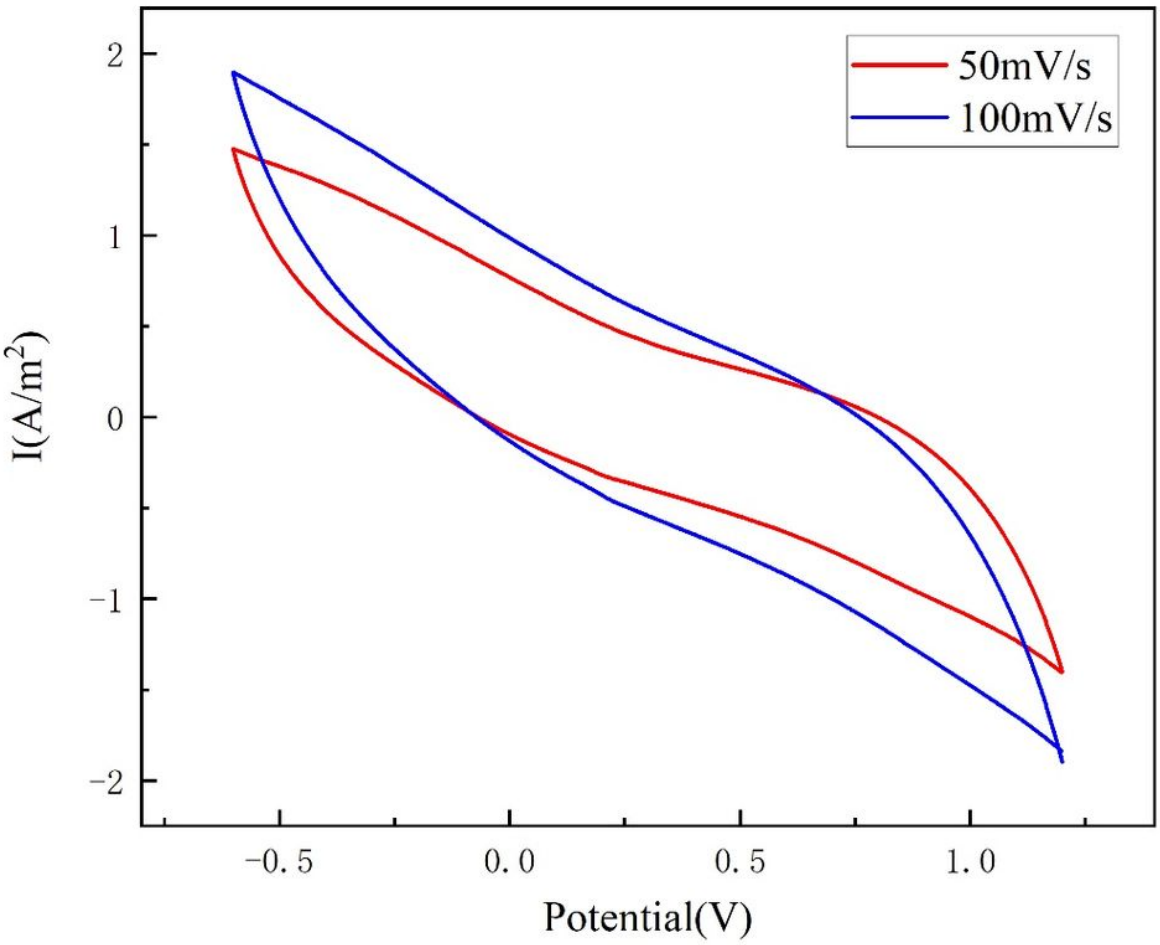

Figure 4

FT-IR spectrum of activated carbon sponge

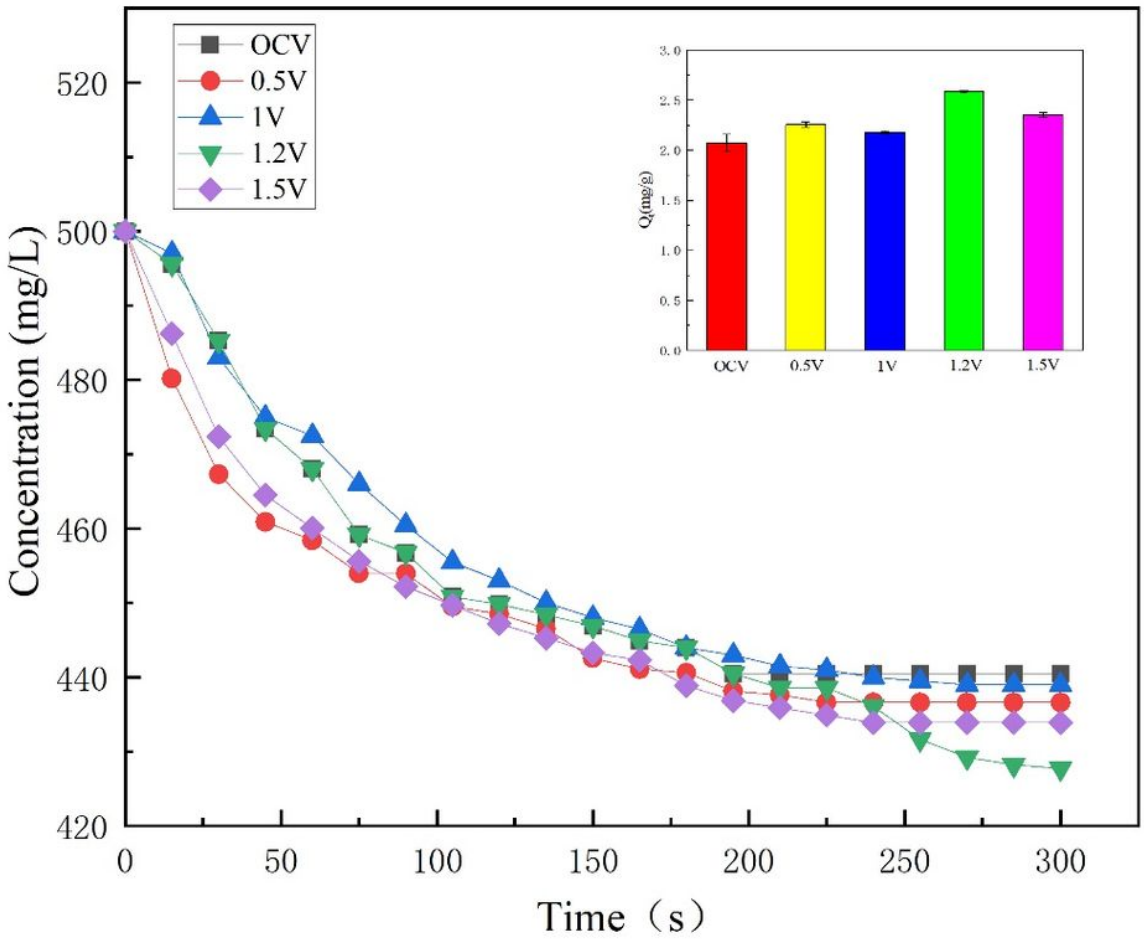

Figure 5

CV curves for sweep velocities of 50 mV/s and 100 mV/s in 1M NaCl solution

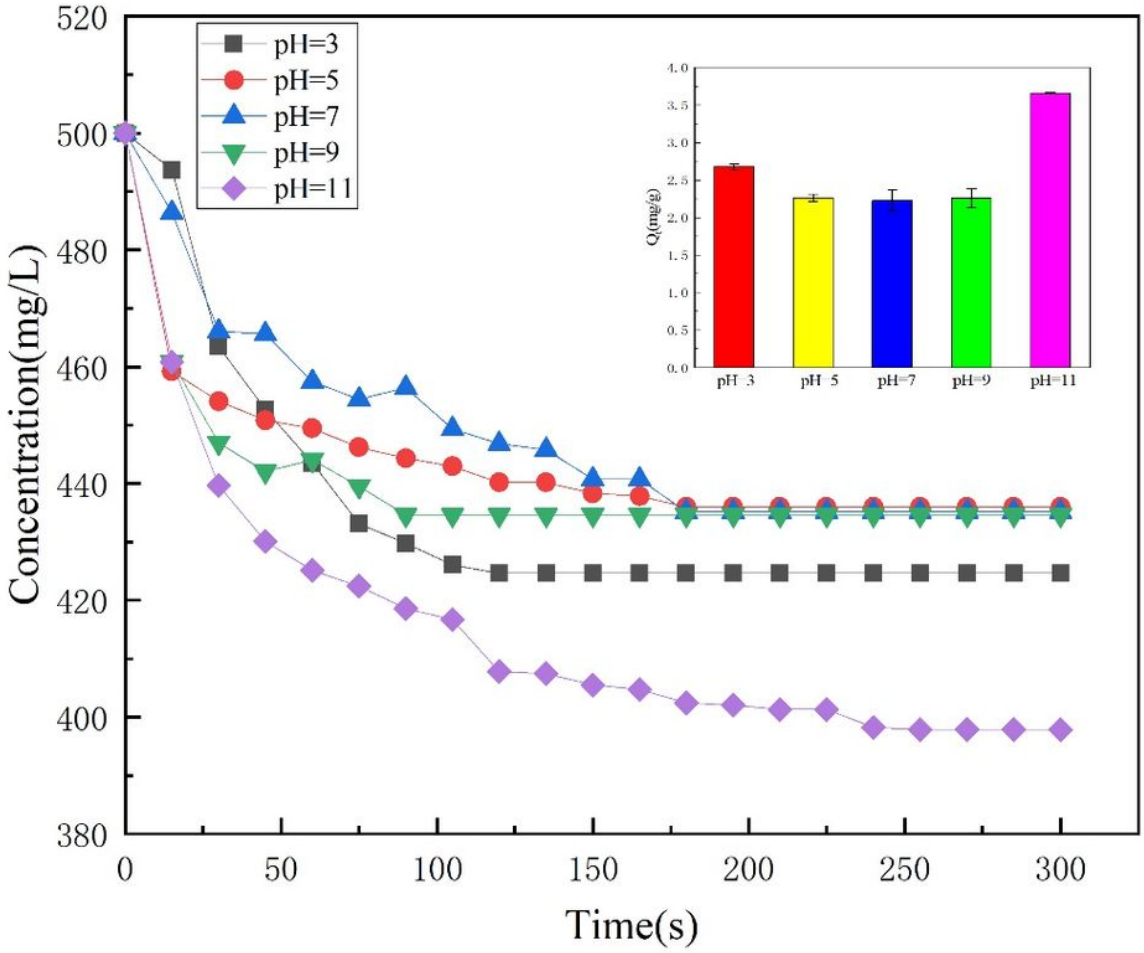

Figure 6

Electrical adsorption performance at different voltages and electrical adsorption capacity at equilibrium

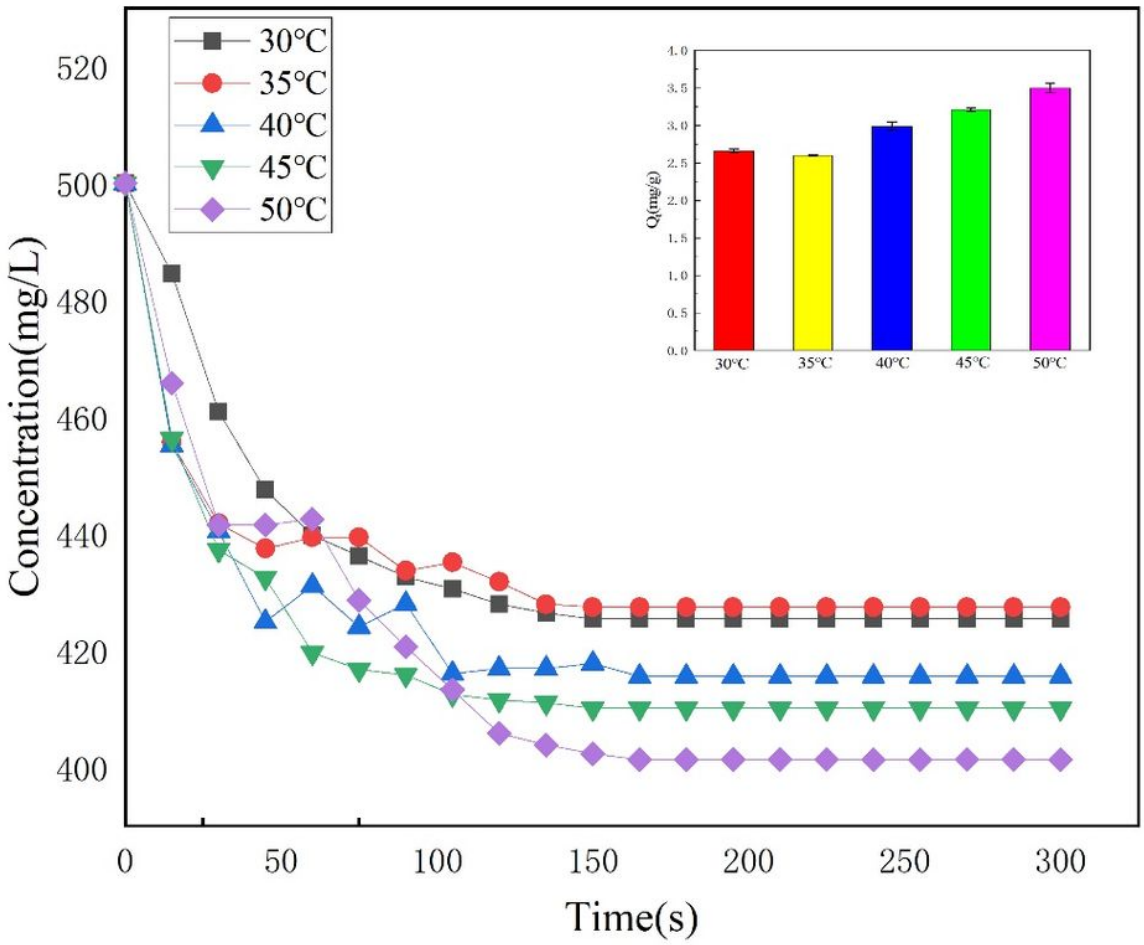

Figure 7

Electrical adsorption performance at different pH and electrical adsorption capacity at equilibrium

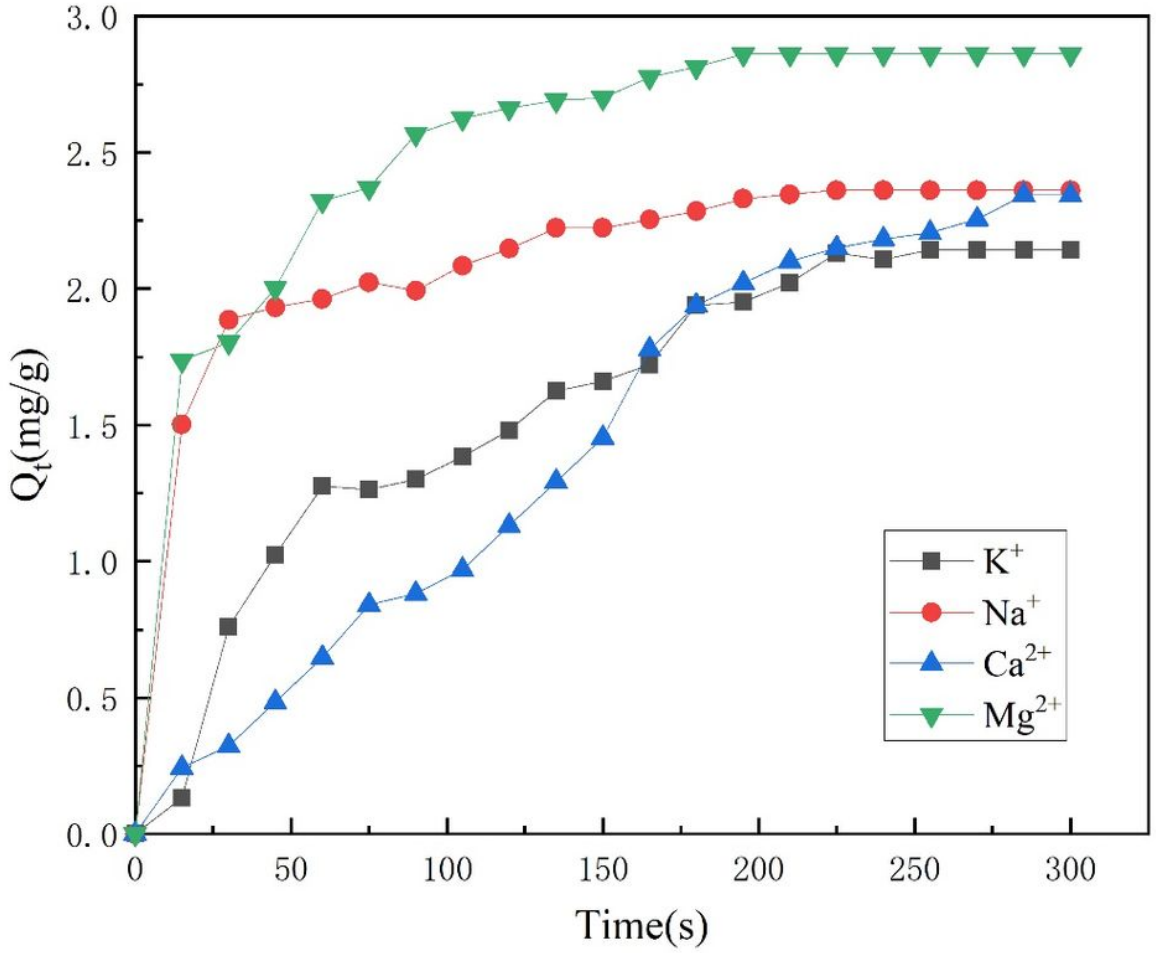

Figure 8

Electrical adsorption performance at different temperature and electrical adsorption capacity at equilibrium

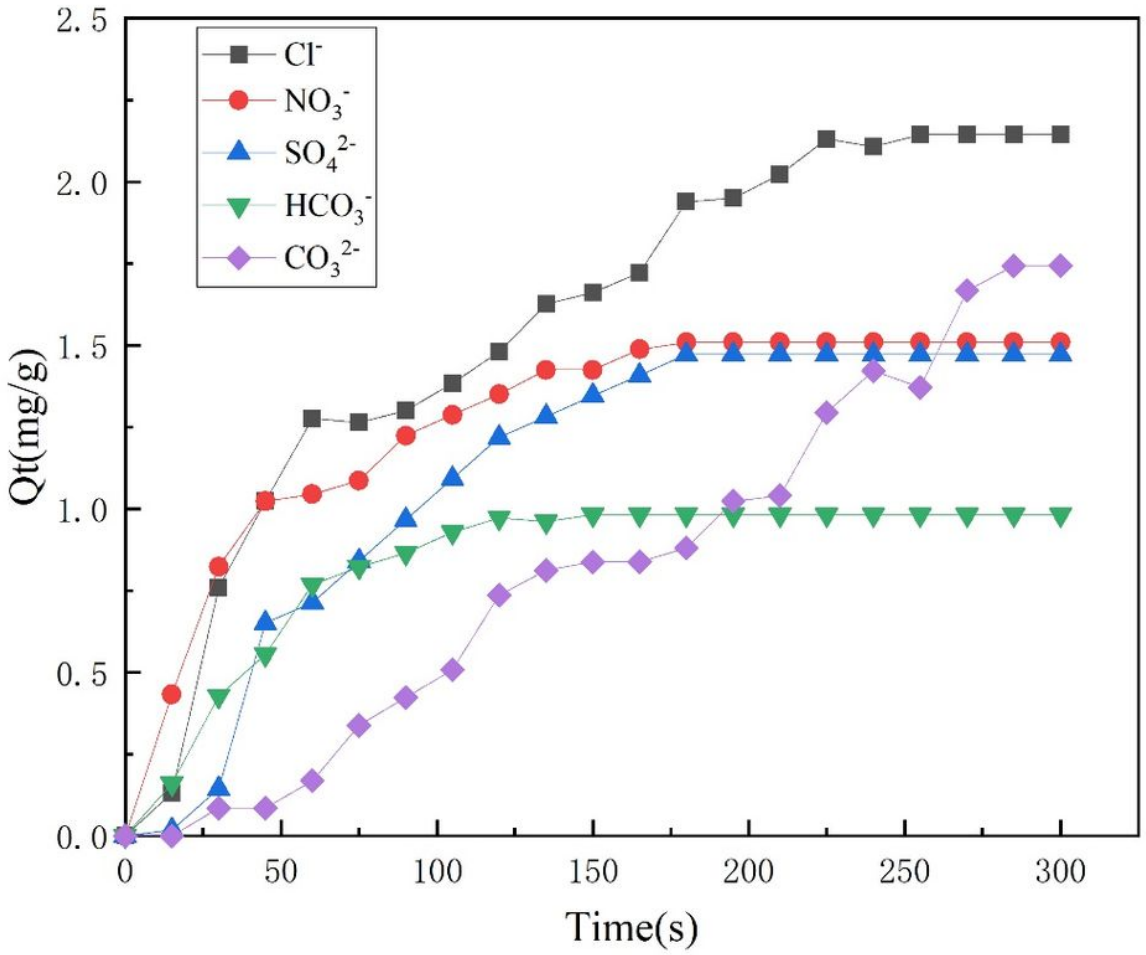

Figure 9

Adsorption capacity curves for different cations treated with CDI

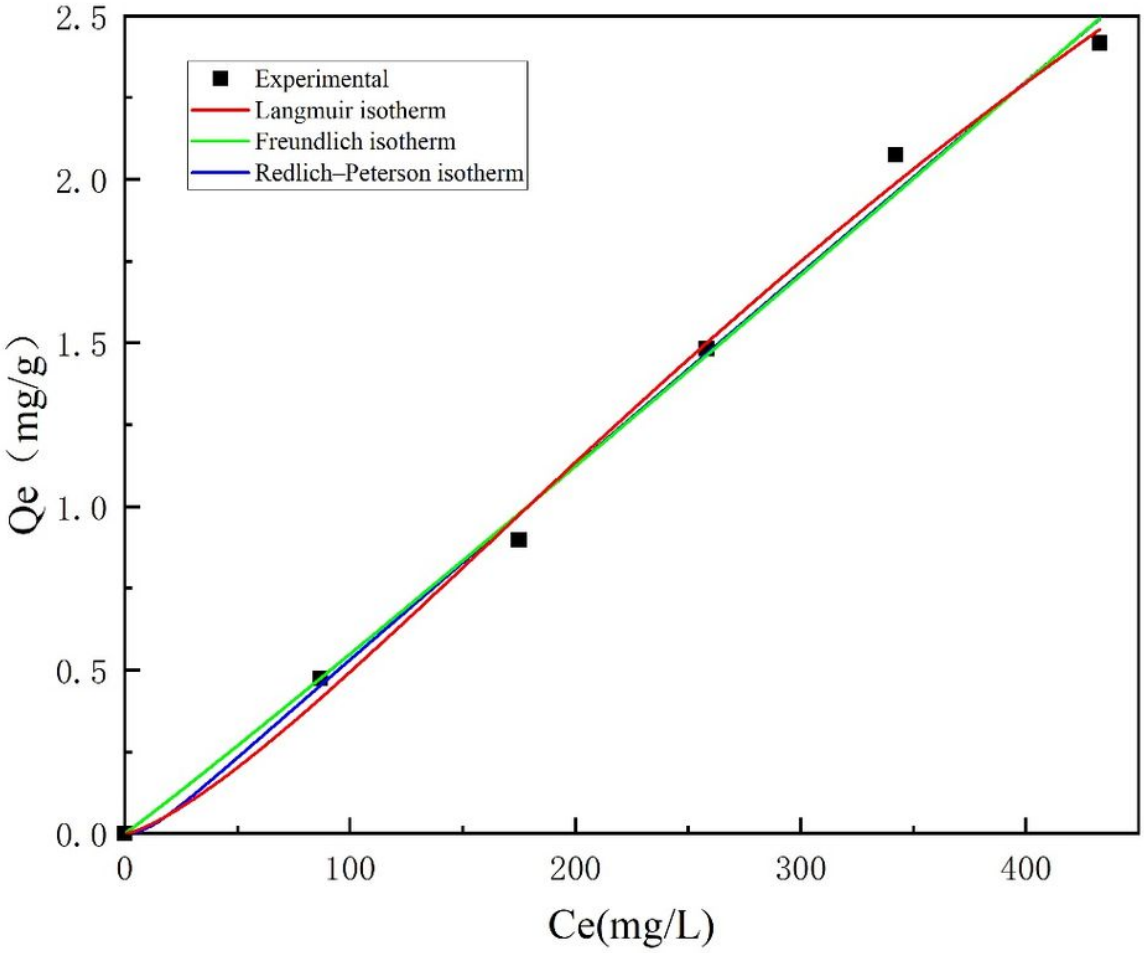

Figure 10

Adsorption capacity curves for different anions treated with CDI

1.1

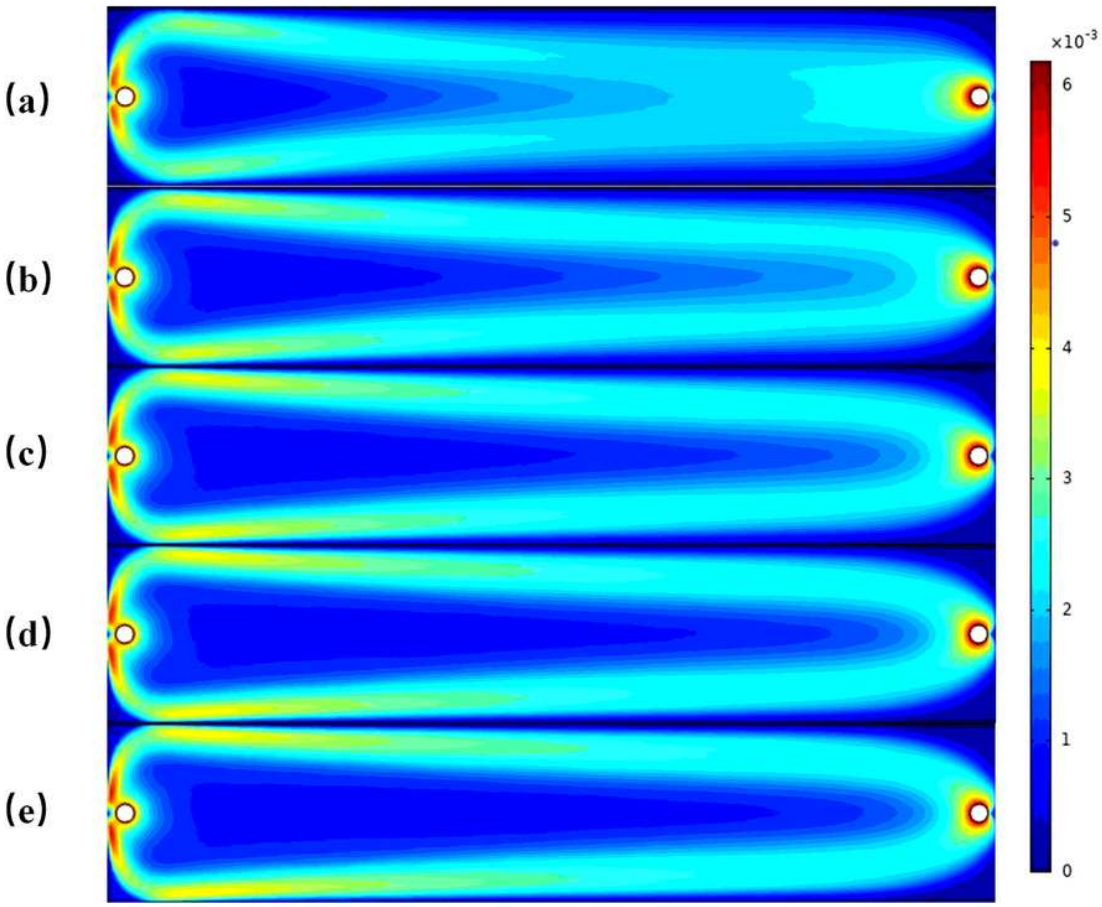

Figure 11

Comparison of kinetic model and experimental data

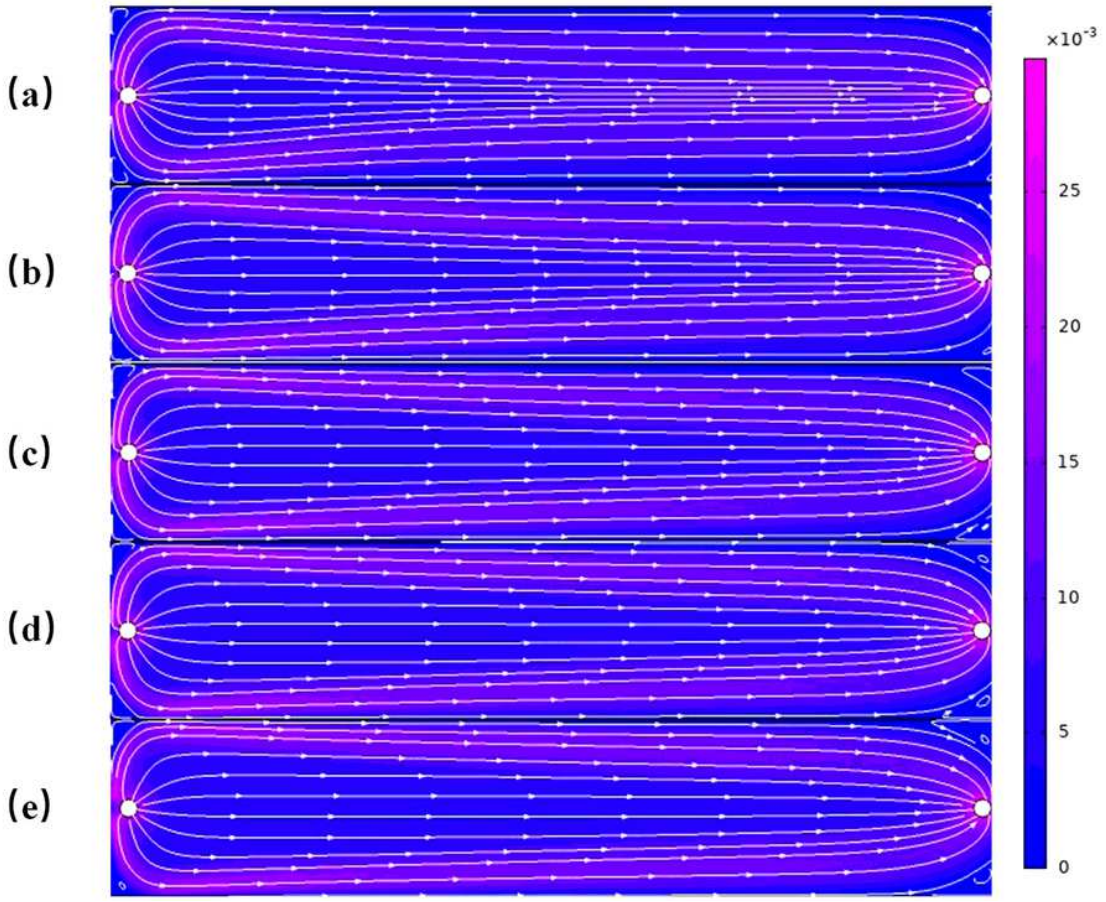

Figure 12

Comparison of three adsorption isotherm models

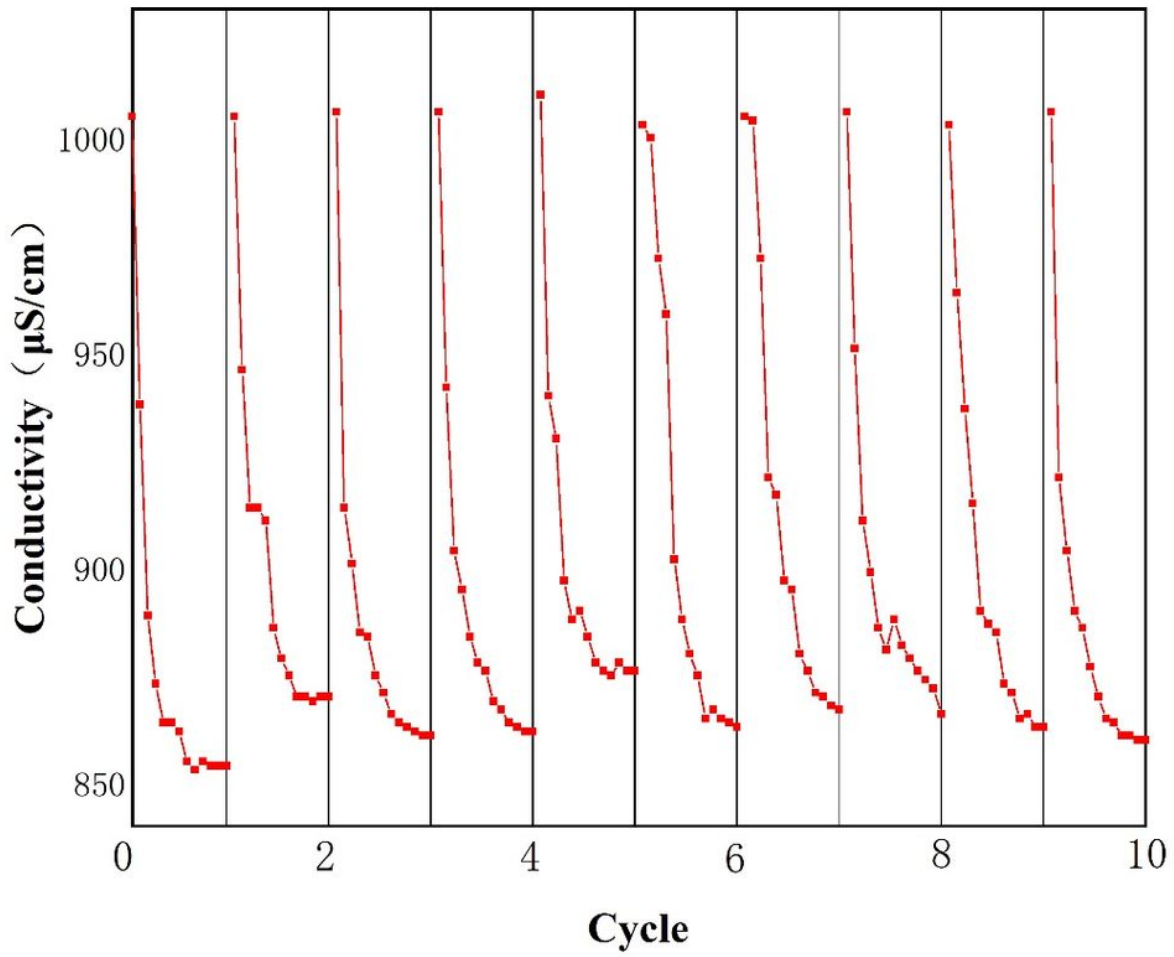

Figure 13

Velocity profiles of rectangular CDI flow paths at different flow rates: (a) 100mL/min, (b) 200mL/min, (c) 300mL/min, (d) 400mL/min, and (e) 500mL/min

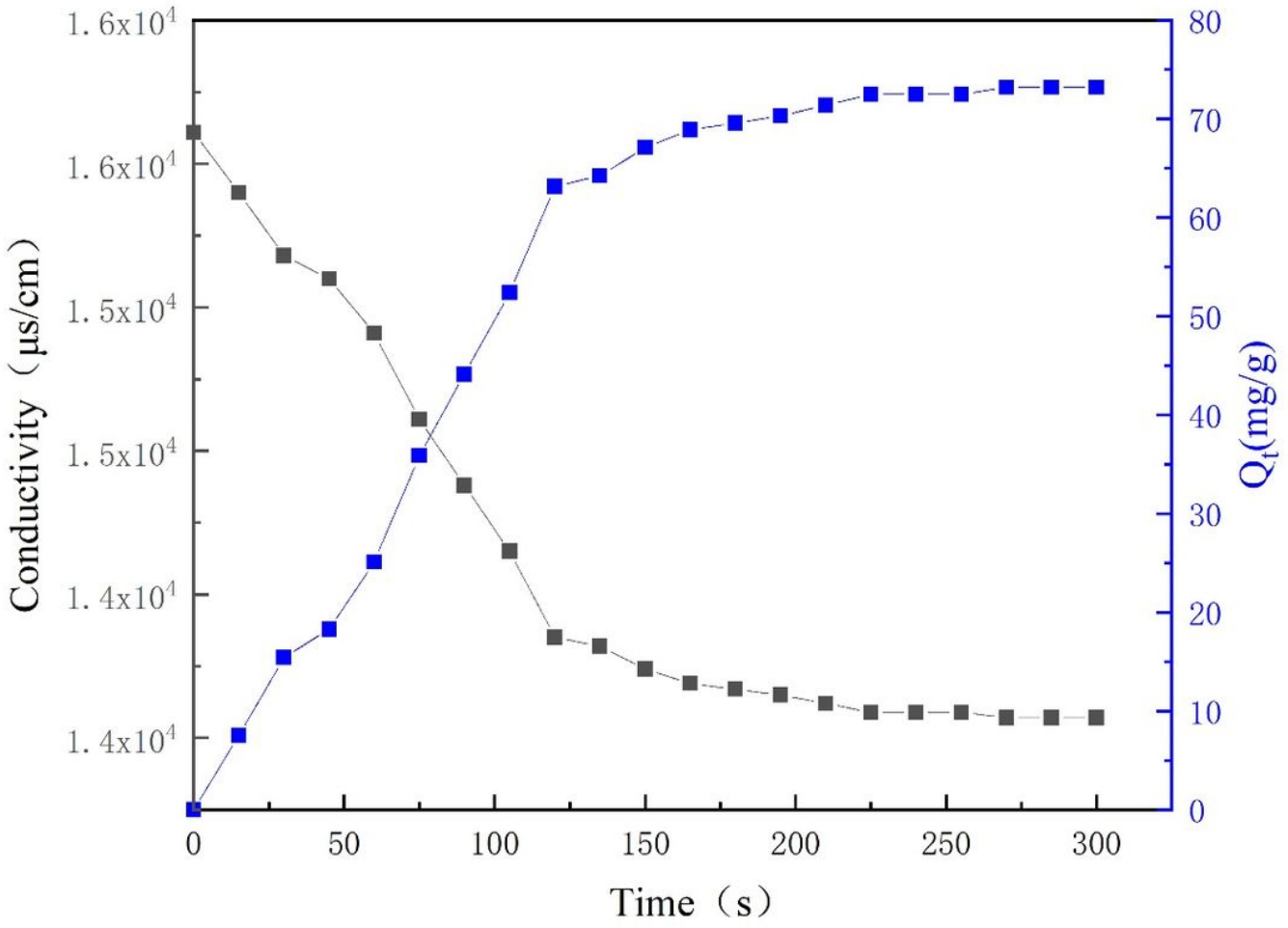

Figure 14

Streamlines profile of rectangular CDI flow paths at different flow rates: (a) 100mL/min, (b) 200mL/min, (c) 300mL/min, (d) 400mL/min, (e) 500mL/min

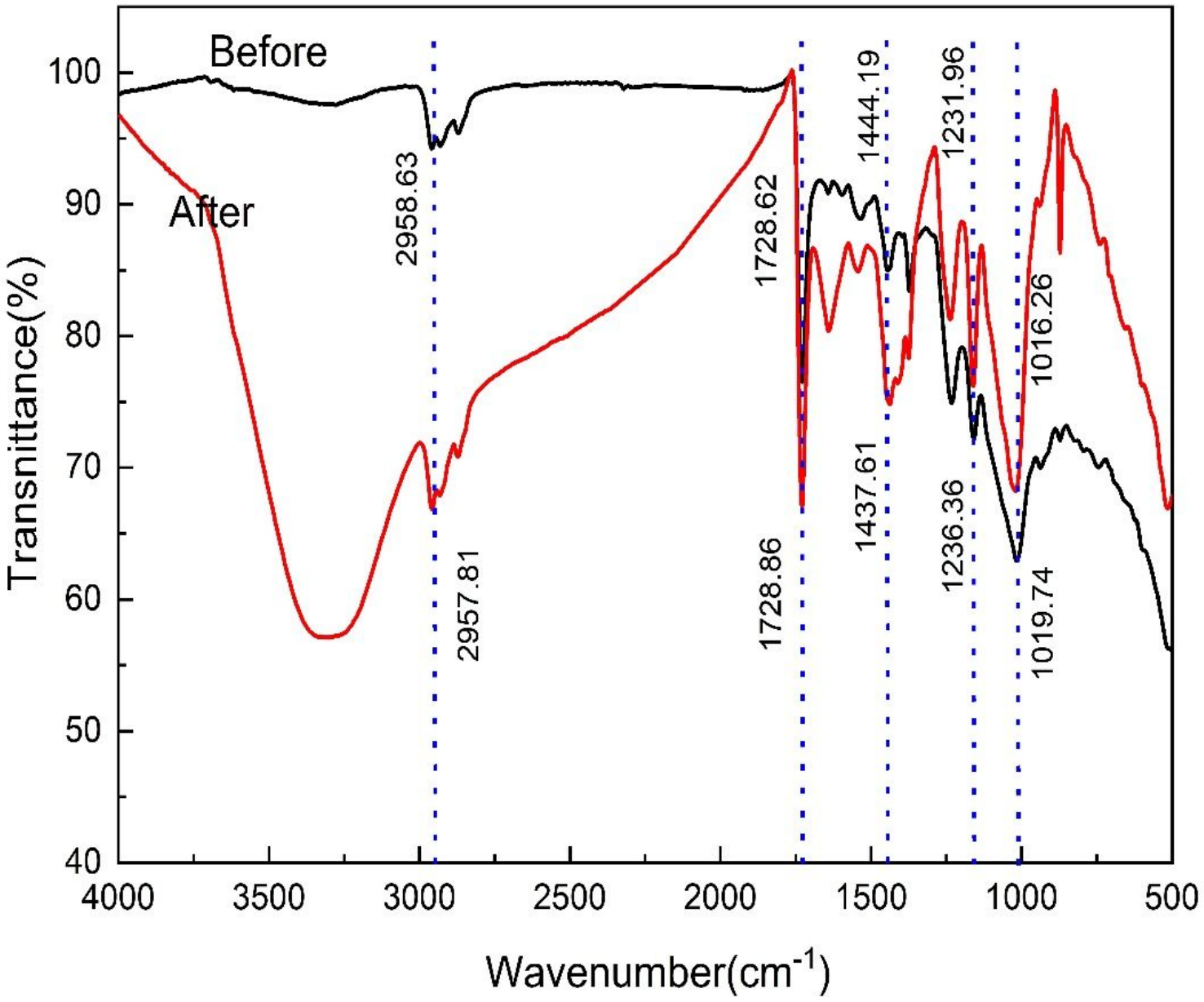

Figure 15

Electrical adsorption performance of CDI unit during 10 cycles

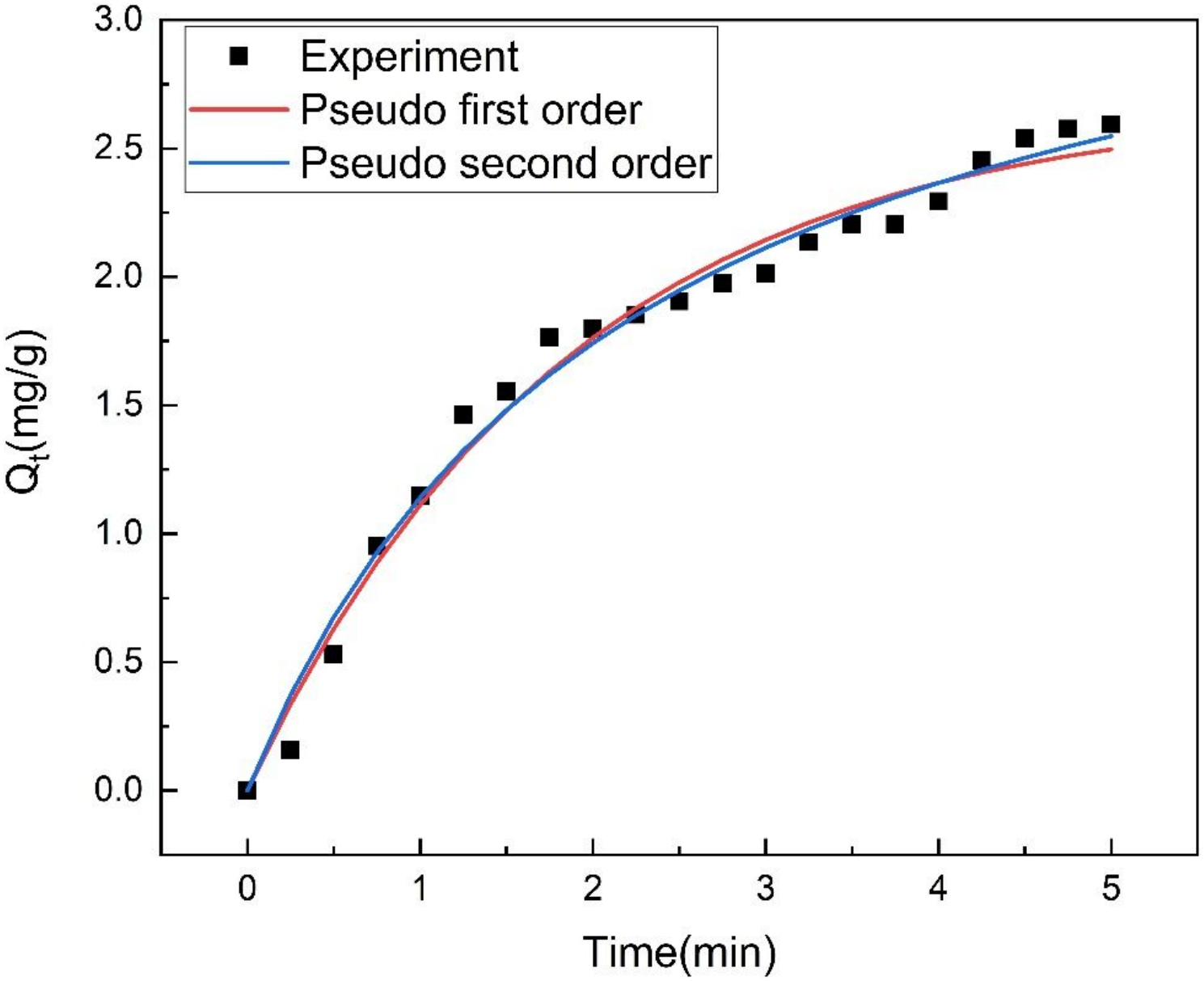

Figure 16

Conductivity and electrical adsorption capacity of CDI treatment of actual desulfurization wastewater

Supplementary Files

This is a list of supplementary files associated with this preprint. Click to download.

- GraphicalAbstract.pdf